Numerical simulation of the edge stress singularity, the edge detachment stress intensity factor and the adhesion strength for compliant mushroom fibrils adhered to rigid substrates

R.G. Balijepalli [ab], M.R. Begley [c], N.A. Fleck [ad], R.M. McMeeking [ace], and E. Arzt [ab]

a INM – Leibniz Institute for New Materials, Campus D2 2, Saarbrücken, Germany

b Saarland University, Campus D2 2, Saarbrücken, Germany

c Materials and Mechanical Engineering Departments, University of California, Santa Barbara, CA 93106, USA

d Engineering Department, University of Cambridge, Trumpington Street, Cambridge CB2 1PZ, UK

e Engineering School, University of Aberdeen, King's College, Aberdeen AB24 3UE, UK

Abstract

Bio-inspired adhesion of micropatterned surfaces due to intermolecular interactions has attracted much research interest over the last decade. Experiments show that the best adhesion is achieved with compliant "mushroom"-shaped fibrils. This paper analyses numerically the effects of different mushroom shapes on adhesion to a rigid substrate. When a remote stress is applied on the free end of a fibril perfectly bonded to a rigid substrate, the resultant stress distribution along the fibril is found to change dramatically between the straight punch and mushroom fibrils. A singular stress field is present at the edge of the fibril where it contacts the substrate and, in this work, the amplitude of the singularity is evaluated for fibrils perfectly bonded to a flat substrate so that sliding cannot occur there. This exercise is carried out for fibril geometries involving combinations of different diameters and thicknesses of the mushroom cap. By assuming a pre-existing detachment length at the corner where the stress singularity lies, we predict the adhesive strength for various mushroom cap shapes. Our study shows that a smaller stalk diameter and a thinner mushroom cap lead to higher adhesive strengths. A limited number of results are also given for other shapes, including those having a fillet radius connecting the stalk

to the cap, and for fibrils having conical mushroom caps. The results support the rational optimization of synthetic micropatterned adhesives.

Key words: fibrils, adhesion, contact mechanics, gecko, finite element modelling.

1 Introduction

Animals in nature possess different hairy contact structures such as straight punches, spherical and conical caps, toroidal suction cups, etc. The climbing abilities of geckos have inspired many researchers to develop reusable, reversible adhesives. Gecko feet are covered with millions of hierarchically structured hairs or setae with sizes ranging from millimetres to nanometres (1-3). The smallest level of hierarchical structure is patterned with finer fibrils; these observations suggest that finer fibrils are associated with better adhesion (4). This insight has led to formulation of the concept of "contact splitting" (4). The present group (5-9), as well as Autumn et al. (10-12) and Jagota et al. (13, 14) have done extensive research on this topic to understand the mechanism behind gecko adhesion. Experiments reveal that either intermolecular van der Waals forces (10) or capillary forces (5) play a major role in the adhesion mechanism.

Polydimethylsiloxane (PDMS) is one of the most widely used materials for the fabrication of gecko inspired adhesives. PDMS has a Poisson's ratio close to 0.5 and a Young's modulus ranging from approximately 100 kPa to approximately 10 MPa, depending on the amount of crosslinking. It is chemically inert, non-toxic and during preparation hardens quickly at elevated temperatures. It has been experimentally proven that PDMS surfaces patterned with fibrils offer better adhesion against a stiff smooth substrate than an unpatterned PDMS surface (15-18).

Experiments with artificial patterned structures have shown that contact cap shape plays an important role in improving adhesion; compared to several different contact geometries, the mushroom fibril has generally been found to adhere best (18-21). Adhesion also depends on other phenomena such as structural instability due to fibril buckling when they are compressed axially (22), misalignment of the adhering surfaces (23), surface roughness (8, 24-26) and backing layer thickness (27, 28). In most of the experiments exploring the adhesion of such patterned surfaces, compliant fibrils are pressed against a stiff spherical substrate and adhesive strength is measured during subsequent tensile loading. The fabrication and experimental exploration of such synthetic

adhesives at the micrometre and nanometre scale are well established in the laboratory setting, and different parameters such as structure aspect ratio, fibril size and cap shape are well investigated. However, there is still a lack of the theoretical models required for a better understanding of the adhesive interactions. The purpose of the present paper is to fill some of the gaps.

There have been on-going efforts by several researchers in the past years to understand the details of gecko adhesion through the development of various analytical models (17, 29-32) and numerical simulations (33-37). Spuskanyuk et al. (33) addressed the influence of shape on adhesion and detailed the reason why mushroom fibrils show better performance than simple punch shapes. Aksak et al. (34) demonstrated the influence of mushroom aspect ratio on adhesion, and Aksak et al. (35) used a Dugdale cohesive zone model for mushroom like fibrils to predict the optimal shape for adhesion. They found that adhesion depends on the edge angle and the ratio of stalk radius to the outer fibril radius. Carbone and Pierro (36) have calculated the dependence of adhesive performance on the mushroom cap geometry and suggested an optimal shape for adhesion. Khaderi et al. (37) provided a detailed analysis of the corner stress singularity at the edge of the fibril, its influence on the stress intensity factor for a small interface detachment near that edge, and the resulting influence on the detachment strength for a single compliant flat bottomed cylindrical fibril attached to a compliant or rigid substrate.

In this work, we consider the corner stress singularity at the edge of a perfectly bonded compliant mushroom fibril on a rigid substrate where sliding of the fibril relative to the substrate is forbidden. In particular, we investigate how the mushroom cap geometry, including its thickness and diameter, influences the adhesive strength. We follow the approach introduced by Akisanya and Fleck (38) to describe the corner stress singularity to explore the mechanics of detachment of $2D$ and $3D$ fibrils, thus extending the work of Khaderi et al. (37) to mushroom caps. To evaluate the parameters of the corner stress singularity, we use finite element analysis, utilizing the commercial finite element software Abaqus (39), to solve for the stresses, strains and deformations in compliant fibrils adhered to a rigid substrate as shown in Figure 1.

2 Analytical solution for the corner singularity

We consider a compliant fibril adhered to a rigid substrate without any interfacial crack. The fibril is treated as an incompressible, isotropic elastic solid, and the edge of the fibril always meets the substrate at right angles. The fibril material is forbidden to slide on the substrate at the interface between them. The boundary condition on the compliant material at the interface with the substrate is therefore one where the displacement is zero. When a tensile load is applied to the fibril as shown in Figure 1, there will be a stress singularity at the fibril edge where it touches the substrate (38). We treat both a straight punch fibril without (Figure 1(a)) and with a mushroom cap (Figure 1(b)). In the current paper we focus on this corner stress singularity to determine its strength and amplitude for the fibrils (straight punch and mushroom shape) shown in Figure 1. Studies have been performed both for plane strain ($2D$) and axisymmetric cylindrical ($3D$) geometries. In addition, we provide a few results for a variation on the shape shown in Figure 1.

[Figure 1 will be here]

We adopt the method of Akisanya et al. (38) and Khaderi et al. (37). The most singular terms in the asymptotic normal (σ_{22}) and shear (σ_{12}) stress components along the interface between a compliant fibril and a rigid substrate (37) are

$$\sigma_{22} = H_1 r^{-0.406} \quad (1)$$

$$\sigma_{12} = 0.505\ \mathrm{H}_1 r^{-0.406} \quad (2)$$

where r is the distance from the fibril edge, and the directions X_1 and X_2 are shown in Figure 1. The amplitude H_1 can be written in terms of the applied stress and one relevant dimension of the fibril. We choose the average stress, σ_I, on the interface between the fibril and the substrate as the measure of the applied stress and the width or diameter, D_f, of the mushroom flange as the relevant dimension and obtain

$$H_1 = \sigma_I D_f^{0.406} \tilde{a} \quad (3)$$

where $\tilde{a}$ is a dimensionless calibration parameter that depends on the geometry of the fibril, including whether it is plane strain or axisymmetric. For a mushroom cap fibril, the average interface stress, σ_I, is written as $\sigma_I = \sigma_A\, D/D_f$ for a plane strain slab and $\sigma_I = \sigma_A \left(D/D_f\right)^2$ for axial symmetry, where σ_A is the stress applied to fibril stalk. Note that when the fibril is a plane strain slab, D_f is the width of the mushroom cap and D is the

width of the stalk, whereas in the axisymmetric cylinder case D_f is the diameter of the mushroom cap and D is the diameter of the stalk. For convenience we will refer to these parameters throughout as the diameter of the mushroom flange and the stalk even when discussing the plane strain results. We note that in the case of a straight punch without a mushroom cap, $D_f = D$, $\sigma_I = \sigma_A$ and $\tilde{a} = a_1$, where the straight punch is illustrated in Figure 1(a), and a_1 is the calibration parameter utilized by Khaderi et al. (37).

In order to verify our computational methods, we repeat the calculations of Khaderi et al (37) for the straight punch attached to a rigid substrate. For the finite element mesh we use a total of 123374 and 100501 linear quadrilateral hybrid elements for plane strain (Abaqus terminology element CPE4RH) and axial symmetry (Abaqus terminology element CAX4RH), respectively. A very fine mesh was used close to the corner of the compliant fibril to increase the accuracy of the results there. The finite element results for the normal and shear stress at the interface are plotted in logarithmic form (base 10) in Figure 2 for both the plane strain and axisymmetric cases and marked "FEM". According to Khaderi et al. (37) $a_1 = 0.331$ for the plane strain punch and $a_1 = 0.278$ for the axisymmetric one. In logarithmic form (base 10), the asymptotic solutions for the plane strain case is thus

$$\log(\sigma_{22}/\sigma_A) = -0.480 - 0.406\, log\, (r/D)$$

and

$$\log(\sigma_{12}/\sigma_A) = -0.777 - 0.406\, log\, (r/D).$$

For axial symmetry it is

$$\log(\sigma_{22}/\sigma_A) = -0.556 - 0.406\, log\, (r/D)$$

and

$$\log(\sigma_{12}/\sigma_A) = -0.853 - 0.406\, log\, (r/D)$$

These 4 results are plotted in Figure 2(a) for plane strain and Figure 2(b) for axial symmetry and marked "asymptotic stress." It can be seen that our finite element results agree very well with the asymptotic solution, thereby verifying the accuracy of our computational method.

[Figure 2 will be here]

With our computational method verified, we concentrate on the corner stress singularity for mushroom fibrils. With the mushroom cap diameter, D_f, held fixed we vary the diameter, D, of the fibril stalk to ascertain the influence of the ratio D_f/D. By proceeding in this way we are able to maintain element structure and size in the finite element mesh adjacent to the interface with the rigid substrate, where the accuracy of the results is most important. The same element types are used for mushroom capped fibrils as are utilized for the straight punches, and between 100,000 and 500,000 elements are used in the finite element models. For each value of D the thickness, h, of the mushroom cap is varied and more than 100 geometric configurations are studied through finite element solutions to quantify the amplitude, $\tilde{a}$, of the corner singularity in each case. The mesh close to the edge of the fibril is always very fine, ensuring the accuracy of the information there in the finite element solutions.

2.1 Predicting the adhesive strength

We now postulate that there is a small detachment or defect of length l at the edge of the fibril as seen in Figure 3 such that the corner stress singularity controls its behaviour. This detachment can represent in an approximate manner the presence of an edge radius on the fibril due to the shape of the mould in which the fibril is formed. Such a detachment is equivalent to an interface crack having a stress singularity at its front, characterized by Mode I and Mode II stress intensity factors, K_I and K_{II} respectively, such that on the interface ahead of the detachment tip the leading order asymptotic stresses are given by

[Figure 3 will be here]

$$\sigma_{22} = \frac{K_I}{\sqrt{2\pi\zeta}} \text{ and } \sigma_{12} = \frac{K_{II}}{\sqrt{2\pi\zeta}} \tag{4}$$

where ζ is the distance from the crack tip as shown in Figure 3. The constants necessary to compute the stress intensity factors are adopted from Khaderi et al. (37) and result in

$$K_I = 2.6H_1 l^{0.094} = 2.6\sigma_I D_f^{0.406} \tilde{a} l^{0.094} \tag{5}$$

$$K_{II} = 0.8H_1 l^{0.094} = 0.8\sigma_I D_f^{0.406} \tilde{a} l^{0.094} \tag{6}$$

We thus see that at a given location ahead of the detachment, the normal stress is 3.25 times the shear stress, showing that the detachment process is dominated by tension and is therefore almost a Mode I phenomenon. Upon detachment, the energy release rate is

$$G = \frac{1-v^2}{2E}\,(K_I^2 + K_{II}^2) = \frac{3}{8E}(K_I^2 + K_{II}^2) = \frac{2.8\sigma_I^2 D_f^{0.81} l^{0.19} \tilde{a}^2}{\mathrm{E}} \qquad 7$$

where E is Young's modulus and ν is Poisson's ratio, equal to 0.5 consistent with incompressibility. For detachment initiated at the edge to occur, the energy release rate must be equal to the adhesion energy, W. The value of the latter should be chosen to be consistent with the mode mixity, i.e. the ratio K_{II}/K_I; however, the mixity is the same for all shapes and sizes of fibrils, so the dependence of the adhesion energy on mode mixity will not affect the relative adhesion strength of fibrils having different configurations. Furthermore, since detachment is nearly Mode I, it will be reasonably accurate to use the adhesion energy for purely tensile detachment as the value for W. When we set $G = W$ in equation 7, the stress, σ_I, is then equal to the interface strength, S^I, for edge initiated fibril detachment. This strength is thus given by

$$S^I = \frac{0.6\sqrt{EW}}{D_f^{0.406} l^{0.094} \tilde{a}} \qquad 8$$

The ratio of strengths of fibrils having the same diameter of mushroom cap and the same edge detachment length is therefore inversely proportional to the ratio of amplitudes of their stress singularities at the fibril edge. Specifically, when a straight punch fibril of diameter $D = D_f$ is compared ceteris paribus with one having a mushroom cap of diameter D_f, their strength ratio for edge initiated detachment is given by

$$\frac{S^I}{S^{punch}} = \frac{a_1}{\tilde{a}} \qquad 9$$

where, as noted above, a_1 is the calibration parameter quantified by Khaderi et al. (37) for the straight punch and S^{punch} is the adhesive strength of the straight punch.

3 Results

3.1 Mushroom fibril

Figure 4 depicts the stress distributions at the interface between a rigid substrate and a fibril with a mushroom cap where the cap diameter is twice that of the stalk ($D_f/D = 2$) and the ratio of the mushroom cap thickness to its diameter (h/D_f) is 0.008. Results are shown both for plane strain (Figure 4(a)) and axial symmetry (Figure 4(b)). It is seen that the stresses at the corner are reduced compared to the results in Figure 2 at the same distance from the corner, while higher stress magnitudes now appear close to the centre of the fibril. This latter feature is somewhat misleading as the region near the corner has a stress singularity and thus there are extremely high stresses there, but not apparent on the scale encompassed by Figure 4. Nevertheless, the fact that the stresses at the fibril centre appear to be the largest present when Figure 4 is considered emphasises that the mushroom cap has reduced the amplitude of the corner singularity considerably. Again good agreement with the asymptotic analytical solution (37) is found, except near the fibril centre where the numerical stresses deviate strongly. This indicates that the corner singularity is not dominant at the fibril centre. The calibration coefficient, $\tilde{a}$, is extracted from the finite element stress solutions for the normal stress, σ_{22}, by fitting it to the asymptotic formula in logarithmic (base 10) form $log(\sigma_{22}/\sigma_I) = log\tilde{a} - 0.406\log(r/D_f)$. The particular mushroom fibril shape shown in Figure 4 has calibration coefficient of $\tilde{a} = 1.3 \times 10^{-10}$ for a $2D$ plane strain fibril and $\tilde{a} = 1.6 \times 10^{-10}$ for the $3D$ axisymmetric fibril.

[Figure 4 will be here]

3.1.1 Varying the mushroom stalk diameter *D*

Figure 5 shows the results for the influence of the mushroom cap diameter, D_f, relative to the stalk diameter, D, when $h/D_f = 0.008$ for axisymmetric fibrils. The equivalent plane strain results are given in the supplementary material in Figure S1. In the calculations, the mushroom diameter D_f (which defines the contact area) is kept constant and D is varied to obtain a range from $D_f/D = 1.09$ to 2. Even for the smallest mushroom cap a significant reduction of the corner stress singularity over the straight punch is found. As the mushroom cap diameter is increased, the magnitude of the corner stress diminishes. Further increases in the mushroom diameter beyond twice the stalk diameter result in further reductions of the corner stress over many orders of magnitude.

[Figure 5 will be here]

3.1.2 Varying cap thickness h

The influence of the mushroom cap thickness h is reported for ten different values for axisymmetric fibrils in Figure 6 when $D_f/D = 2$. The plane strain results are given in the supplementary material in Figure S2. Again, the mushroom diameter is kept constant and h is varied. It is observed that the amplitude of the corner stress singularity decreases when h/D_f decreases. The corner stress for thin caps, e.g. $h/D_f = 0.008$, is very low and the maximum stress visible in the plots lies close to the centre of the fibril. Any increase in h/D_f increases the corner stress, which approaches that of a straight punch as h increases.

[Figure 6 will be here]

Figure 7 shows the calibration coefficient $\tilde{a}$ plotted versus h/D_f for various values of D_f/D for plane strain (Figure 7(a)) and axisymmetric (Figure 7(b)) mushroom fibrils. In addition, the results for straight punch fibrils are shown on the plots as horizontal dashed lines. On increase of the stalk diameter D and the mushroom cap thickness h the calibration coefficient $\tilde{a}$ increases and approaches the value for that of a straight punch, i.e. 0.331 for plane strain and 0.278 for the axisymmetric case. Figure 8 similarly depicts the calibration coefficient $\tilde{a}$ as a function of the thickness, h, for fibrils having mushroom caps for axial symmetry, but now up to cap thicknesses that are comparable to the diameter of the mushroom cap. The result for a straight punch is also shown as the horizontal dashed line. This plot clearly shows that as the mushroom cap becomes very thick, and therefore the lower segment of the fibril becomes indistinguishable from a straight punch, the behaviour reverts to that of the straight punch.

We have compiled all values of the calibration coefficients from our results and presented them in Table 1 and Table 2.

[Figure 7 will be here]

[Figure 8 will be here]

[Table 1and Table 2 will be here]

3.2 Adhesion strength

The adhesion strength controlled by edge initiated detachment for fibrils having mushroom caps was next calculated by using equation 9 so that the strength is normalised by that of a straight punch where both the fibril with the mushroom cap and the straight punch have the same diameter where they contact the substrate, the same detachment length, l, at the corner, the same Young's modulus and the same adhesion energy, W. That is, the diameter of the mushroom fibril cap is the same as the diameter of the straight punch. We note that the detachment length l is small ($l \ll D_f$) so that its behaviour is controlled by the corner singularity. The results for adhesion strength are shown in Figure 9 for both plane strain (Figure 9(a)) and axisymmetric (Figure 9(b)) fibrils, and are shown as functions of h/D_f for various values of D_f/D. The results for straight punches are shown as horizontal dashed lines.

It is observed that the fibril cap geometry plays an important role in promoting adhesive strength. As the mushroom cap diameter is increased and as the cap thickness is decreased, the adhesive strength rises. Therefore, both a thin mushroom cap and one with a large diameter enhance the adhesive strength of the fibril when strength is controlled by detachment from a defect at the corner. In fact we observe that the adhesive strength can be enhanced by 10 orders of magnitude over the straight punch strength S^{punch} when the mushroom cap diameter is twice that of its fibril stalk and its thickness is less than 1% of its diameter.

[Figure 9 will be here]

We note, however, that the benefit from the mushroom cap is limited by 3 sources. One source of the limitation is the inherent strength of the bond between the fibril and the substrate, which can lead to detachment commencing near the centre of the fibril rather than at the edge. The second source is that weak areas of bonding or of no bonding at all may be present near the centre of the fibril, representing adhesion defects that may initiate detachment. The third source of limitation is the strength of the fibril material itself, which may lead to the stalk of the fibril rupturing, since the mushroom shape leads to a stress in the stalk that is higher than the average stress at the interface with the substrate. In the current work we have not addressed the material strength. Therefore, we cannot qualify our results with quantified limits from this source. However, the inherent strength of the bond between the fibril and the substrate can be addressed based on the following consideration. We observe from Figure 4, 5 and others that the stress at the interface for

the mushroom fibril is almost uniform under the stalk. When the stress at that location reaches a critical value, S^C, we assume that the cohesive strength of the bond has been reached and detachment of the fibril occurs, if it has not already occurred through an alternative mechanism, such as propagation of the defect at the edge of the contact. Furthermore, detachment motivated by an adhesion defect at or near the centre of interface between the fibril may be considered explicitly and this is addressed below; in this case we consider an adhesion defect located at the peak stress visible in Figures 4 & 5 just below the edge of the stalk of the fibril.

We now assume that detachment can occur by one of the three failure modes just described, namely that triggered when stress at the interface under the stalk reaches the critical value S^C. In Figure 10 for comparison with this critical stress the adhesion strength, S^S, for fibrils having mushroom caps is shown in terms of the average stress on the mushroom fibril stalk instead of the average stress on the interface. The results are normalised by the adhesion strength of a straight punch fibril, S^{punch}, having the same diameter as the mushroom cap, and the same edge detachment length, Young's modulus and adhesion energy, and are shown for plane strain in Figure 10(a) and for axial symmetry in Figure 10(b). Results for straight punches are shown as full horizontal lines. The detachment strength associated with the stress under the stalk reaching the critical level S^C is shown as a horizontal dashed line marked "cohesive strength S^C" in the figure legend. The location of this dashed line on the ordinate is arbitrary as we do not select a specific value of the cohesive strength for any given interface. Thus the line can be adjusted up or down to represent the cohesive strength in any given case; however, in plotting the dashed lines in Figure 10 we have assumed that the cohesive strength of the interface exceeds the strength of straight punches when detachment in that case initiates at the corner. The dashed line in Figure 10 is to be used in the following manner. The detachment strength for mushroom fibrils cannot exceed the value represented by the dashed line; therefore, for any given combination of mushroom cap diameter and thickness, the detachment strength is given by the lower of the dashed line and the line representing the fibril detachment strength when detachment initiates at the corner of the mushroom cap. We conclude, therefore, that given our assumption regarding the cohesive strength behaviour, fibrils with very thin, large diameter mushroom caps will experience detachment that initiates near the centre of the fibril, and will have a detachment strength predicted approximately by the horizontal dashed lines in Figure 10. In contrast, fibrils

having thick, small diameter mushroom caps will experience detachment that initiates at the edge and their adhesive strength will be predicted by the full lines in Figure 10.

[Figure 10 will be here]

When we inspect Figure 5 and Figure 6 we note that there is a peak in the normal traction at the interface that is located approximately under the edge of the fibril stalk. It is possible that the high stress under the edge of the fibril stalk will exceed the cohesive strength of the interface and therefore can initiate fibril detachment. Furthermore, if a detachment defect in the form of a region that is not adhered is located there it is possible that fibril detachment will initiate due to that defect. To further characterise this possibility, in Figure 11 we have plotted the ratio of the peak stress, σ_{Peak}, to the average interface stress σ_I, as a function of h/D_f, for various values of D_f/D for axially symmetric fibrils having mushroom caps. It is convenient at this point to introduce the notation of a stress concentration factor for the stress at the interface under the edge of the fibril stalk as $k = \sigma_{peak}/\sigma_I$.

We note that as the mushroom cap is made thinner or its diameter is made larger the peak in stress under the edge of the fibril stalk becomes more pronounced, and is more likely to promote fibril detachment. Therefore, the influence of this peak in stress on the likelihood of fibrillar detachment runs counter to that of the effect of the mushroom cap on edge detachment, whose likelihood is diminished by a thin, large diameter mushroom cap.

The influence of the peak in stress plotted in Figure 11 may be investigated as follows. As a rudimentary treatment of the relevant fracture mechanics, we may consider a small detachment of length or diameter $2a$ at the location of the peak stress. There will be a stress singularity around the edge of this detachment that will control the tendency for it to spread. As an approximation we may estimate this stress intensity factor as if the detachment were present in an infinite body subject to a stress equal in magnitude to the peak in stress plotted in Figure 11. The resulting value is

$$K_I = \sigma_{peak}\sqrt{\pi a} \qquad 10$$

Note that we have not attempted to estimate a shape factor that would multiply the right hand side of equation 10 but instead have simply assumed that this factor is unity. As our treatment is highly approximate, we consider this to be satisfactory. With K_{II} assumed to be zero, we compute the energy release rate according to the first and second results on

the right hand side of equation 7 and set it equal to the adhesion energy to predict fibril detachment initiated as such a defect. The predicted strength, S^P, in terms of the average interface stress, for fibril detachment initiated at a defect at the location of the peak stress is then

$$S^P = \frac{1}{k}\sqrt{\frac{8EW}{3pa}} \qquad 11$$

where k is the stress concentration factor for the peak stress as introduced above in connection with Figure 11.

The competition between detachment initiated at the edge of the mushroom cap and that initiated at a defect at the location of the peak stress under the edge of the fibril stalk is explored in Figure 12 as follows. The non-dimensional strength for edge detachment follows directly from Eq. 8 as

$$\overline{S}^I = \frac{S^I D_f^{0.406} l^{0.094}}{0.6\sqrt{EW}} = \frac{1}{\tilde{a}} \qquad 12$$

From Eq. 11 the strength for fibril detachment initiated at a defect located at the peak stress under the edge of the fibril stalk is now expressed in this non-dimensional form as

$$\overline{S}^P = \frac{S^P D_f^{0.406} l^{0.094}}{0.6\sqrt{EW}} = \frac{D_f^{0.406} l^{0.094}}{0.3k\sqrt{1.5pa}} \qquad 13$$

A comparison of $\overline{S}^I$ and $\overline{S}^P$ is plotted in Figure 12. The curves for $\overline{S}^P$ are marked "Detachment caused by a defect at the location of high stress under the edge of the fibril stalk." Note that for illustration we have chosen three different values for $3.3D_f^{0.406} l^{0.094} / \sqrt{1.5\pi a}$ namely $50, 100$ &, 200, representing the relative sizes of the two defects of length l and $2a$ respectively and the diameter, D_f, of the mushroom cap. These curves are marked in Figure 12 by their values $50, 100$ &, 200 respectively. These choices of $50, 100$ &, 200 are somewhat arbitrary and the reason for them will become clear below.

[Figure 11 will be here]

[Figure 12 will be here]

In Figure 12 the curve for $\overline{S}^I$ is marked "Detachment caused by a defect at the edge of the mushroom cap." It can be seen that with the chosen relative sizes of the defects the plot for edge initiated detachment, within the domain of the figure, intersects with the plots for detachment commencing at the location of the peak stress. This is the reason for choosing the values $3.3D_f^{0.406}l^{0.094}/\sqrt{1.5\pi a} = 50, 100$ & 200 as the resulting intersections enable us to illustrate the relevant situation, which is as follows. For this explanation we focus on the case where either edge initiated detachment takes place or detachment occurs commencing at the location of peak stress with flaw sizes such that $3.3D_f^{0.406}l^{0.094}/\sqrt{1.5\pi a} = 200$. In this case, the adhesive strength of the fibril is predicted by the lower of the curve for the latter and the curve for edge initiated detachment in Figure 12. This implies that for small values of h/D_f detachment will be initiated at the defect under the peak in stress at the edge of the fibril stalk, whereas for large values of h/D_f detachment will be initiated at the edge of the mushroom cap. The reason for choosing the three different values $3.3D_f^{0.406}l^{0.094}/\sqrt{1.5\pi a} = 50, 100$ & 200 in Figure 12 is to illustrate how the domains of edge initiated detachment and detachment initiated at the peak stress location vary as the relative sizes of a, l and D_f change. It can be seen that as $3.3D_f^{0.406}l^{0.094}/\sqrt{1.5\pi a}$ becomes larger, the domain in which edge initiated detachment occurs becomes more extensive; this outcome is a consequence of the fact that $3.3D_f^{0.406}l^{0.094}/\sqrt{1.5\pi a}$ becomes larger as a consequence of a diminishing, so that detachment caused by a defect at the location of the peak stress at the edge of the fibril stalk is less likely.

4 Discussion

Spuskanyuk et al. (33) provided the initial study on how the corner stress singularity varies from a straight punch to a mushroom fibril for frictionless and sticking friction conditions. In the course of the work just described we have repeated their simulations and our results are in good agreement with theirs. They also reported how the stress varies along the substrate interface for the straight punch and the mushroom fibril, and a similar

behaviour can be observed in our results in Figure 1, Figure 2 and Figure 4 respectively. The straight punch exhibits lower adhesive strength when compared to mushroom fibrils because the corner stress singularity acts as the driving force to initiate detachment. In the case of the mushroom fibril, the extra material present on either side of the stalk evidently reduces the corner singularity, which in turn improves the adhesive strength of the fibril. The results in Figure 5 and Figure 6 show that there is a zone of higher stress at the centre of the fibril under the edge of the stalk, from where detachment could now initiate. Experimentally, such a behaviour was found by Hossfeld et al. (40) and by Micciché et al. (23), who observed that detachment of mushroom fibrils started from close to the centre. We have only investigated this issue in a preliminary manner as we have not quantified the strength of the adhesive bond between the fibril and the substrate for any specific combination of materials. However, we have provided illustrative results that indicate the trade-off between detachment initiated near the centre of the fibril and that commencing at the edge of the mushroom cap.

The most systematic experimental study on how the contact shape of a compliant PDMS (polydimethylsiloxane) fibril adhered to a glass probe affects adhesion was published by del Campo et al. (19). They examined different geometries such as the straight punch, the spherical cap, the spatula cap, the straight cap with rounded edges, the mushroom cap and the concave cap. Mushroom fibrils showed superior adhesion when compared to other shapes. The adhesive strength of the straight punch and the mushroom fibril varied from approximately 30 to 60 kPa depending on the fibril radius and preload. For a mushroom fibril with $D_f/D = 1.29$, the adhesive strength varied from 30 to 185 kPa.

Carbone and Pierro (36) have calculated the dependence of adhesive performance on the mushroom cap geometry and suggested an optimal shape for adhesion. They erroneously assumed that the corner stress singularity involves inverse square root behaviour, a result that cannot be justified as it disagrees with the analysis of Khaderi et al. (37) and our results. Therefore, their interpretation of their results cannot be deemed to be reliable, as they used the wrong order of singularity throughout their analysis. However, Carbone and Pierro (36) show results for stress at the interface between the fibril and the substrate that can be used in principle to deduce the adhesive strength of mushroom shaped fibrils, albeit of a different design from the ones we have considered. On the other hand, the mushroom caps that Carbone and Pierro (36) consider in their analysis are very large in diameter, with the smallest one having a diameter twice as large as that of the fibril stalk. As we

have shown that mushroom fibrils having cap to stalk diameter ratios much less than 2 are very effective at raising fibril adhesive strengths, the designs contemplated by Carbone and Pierro (36) are somewhat unrealistic and unnecessary.

Aksak et al. (35) have presented a computational study on how the geometry of a wedge or conical shaped mushroom cap influences fibrillar adhesion by varying the angle (from $25°$ to $80°$) at which the wedge shaped mushroom cap meets the substrate to which it is adhered. They used a Dugdale cohesive zone to model the detachment process at the interface between the fibril and the substrate. They found that the strongest adhesion was associated with a mushroom cap that meets the substrate at $45°$ such that the diameter of the contacting surface is 11 % and 12 % larger than the diameter of the stalk of the fibril. They found that adhesive strength fell off if they varied either the contact area or the contact angle away from this case. In addition, in the $45°$ case they appended a thin disc of material to the tip of the fibril where the disc had the same diameter as the fibril tip, thus introducing a $90°$ contact angle and they found that in many cases this compromised the adhesive strength of the fibril.

4.1 Improved shape for a fibril having a mushroom cap

As noted above, the results in Figure 5 and Figure 6 show that there is a peak in the normal traction at the interface between the fibril and the substrate that is located immediately under the edge of the fibril stalk. We have explored designs that will eliminate this elevation in the stress, and have found that it disappears when there is a fillet radius, as in Figure 13, smoothing the transition from the fibril stalk to the mushroom cap. As an example of this improvement in the design, we carry out simulations for the stress at the interface between the substrate and fibrils having $D_f/D = 1.41$ and a fillet radius, R, such that $R/D_f = 0.083$. The results for the normal traction at the interface are shown in Figure 14 for various values of h/D_f for axial symmetry. It can be seen that the stress elevation visible in Figure 5 and Figure 6 is absent in the results in Figure 14. In this case the maximum normal traction under the fibril, other than at the edge of the cap, is simply twice the average stress on the interface.

[Figure 13 will be here]

[Figure 14 will be here]

The calibration coefficient for the edge singularity is extracted from the results in Figure 14 by fitting the plots to the asymptotic solution as before. The results, designated $\tilde{\alpha}_{fillet}$, are shown in Figure 15, as are the calibration coefficients, $\tilde{\alpha}$, for fibrils having mushroom caps without the fillet radius. It can be seen that the introduction of the fillet radius has increased the amplitude of the edge singularity compared to that prevailing in the absence of the fillet radius. It follows that the mushroom fibrils with the fillet radius will be more prone to edge detachment than the equivalent design lacking a fillet radius. However, the fillet radius, by eliminating the peak in stress that would otherwise occur under the edge of the stalk, diminishes the likelihood of detachment commencing near the centre of the fibril.

[Figure 15 will be here]

[Table 3 will be here]

In Figure 16 we have replotted the results in Figure 15 to represent S^I/S^{punch}, the ratio of the adhesive strength of a fibril having a mushroom cap to that of a punch shaped fibril. One curve, marked "With fillet radius" gives the results for fibrils with the fillet radius connecting the mushroom cap and the stalk, while the results marked "Without fillet radius" are for the fibrils lacking the smooth transition from stalk to mushroom cap. It can be seen that the adhesive strength of the fibrils having a fillet radius is somewhat poorer than that for fibrils in which the fillet radius is absent. However, that conclusion is associated with detachment that commences at the edge of the mushroom. Due to the lack of a peak in the stress under the fibril stalk when there is a fillet radius present, the situation will be reversed when detachment commences near the centre of the fibril. In the case of the fibrils used for the calculations with results presented in Figure 16, the adhesive strength for detachment commencing at the centre of the fibril, measured in terms of S^I, i.e. the average stress on the interface, will be $\sigma_o/2$, where σ_o is representative of the cohesive interaction strength between the fibril and the substrate. If we assume that this interaction is of the Dugdale type, σ_o will be equal to the cohesive stress attracting one surface to the other.

[Figure 16 will be here]

In fact, we can assume that a fillet radius can be introduced in all cases to smooth the transition from the fibril stalk to the mushroom cap no matter the values of the ratios

D_f/D and h/D_f. Designs can then always be found with a sufficiently effective fillet radius such that detachment will commence near the centre of the fibril, and this will occur at a strength, measured in terms of the average stress at the interface, given by

$$S^I = \left(\frac{D}{D_f}\right)^2 \sigma_o \qquad 12$$

Thus the best strength is achieved with the smallest possible mushroom cap diameter that eliminates edge detachment and therefore leads to a strength quite close to the cohesive stress.

5 Conclusion

In the current work we focus on the corner singularity for a mushroom fibril that is assumed to be perfectly bonded to a rigid substrate so that no sliding can occur at the interface between the fibril and the substrate to which it is attached. The mushroom cap and stalk dimensions are varied and the calibration coefficient and the adhesive strength are calculated for the resulting combinations of mushroom cap geometry. In total, more than a hundred different combinations of fibril geometry are analysed in this study. The following conclusions can be drawn:

- In agreement with earlier work, straight punch fibrils exhibit a corner stress singularity. This explains the tendency of straight fibrils to detach from a corner location.
- In mushroom fibrils, the corner stress is reduced to a level that may preclude detachment initiating at that location. Instead, the stress near the centre of the fibril may initiate detachment there.
- The mushroom geometry strongly influences the stress distribution. The corner stress singularity amplitude is minimized for small cap thicknesses and small fibril stalk diameters.
- Optimisation of fibrillar adhesives will require mushrooms caps with minimum thickness and minimum stalk diameter, but limited by the tendency for detachment to occur near the centre of the fibril and by the material strength.

- Introduction of a fillet radius to smooth the transition from the fibril stalk to the mushroom cap was successful in removing the stress peak that otherwise occurs in mushroom fibrils on the interface immediately below the edge of the fibril stalk. However, the adhesive strength controlled by the edge singularity is reduced, which is a drawback. However, the adhesive strength associated with detachment commencing near the centre of the fibril is improved. The results suggest that an adhesive strength close to the cohesive stress at the interface can be achieved with careful design of the mushroom cap and the fillet radius. A detailed analysis is necessary to establish the best design.

Acknowledgements:

RB thanks GRADUS, Faculty 8.4. Natural Sciences, of Saarland University for partially funding his research visit to the University of California, Santa Barbara. RB would also thank Dr. S. Khaderi for his help in setting up the model. He also thanks Dr. R. Hensel and Dr. N. Guimard for fruitful discussions and for their continuous support. EA acknowledges funding from the European Research Council under the European Union's Seventh Framework Program (FP/2007-2013)/ERC Advanced Grant no. 340929.

References

1. HILLER U. Untersuchungen zum Feinbau und zur Funktion der Haftborsten von Reptilien, Z Morph Tiere 1968: 62: 307-362.
2. AUTUMN K., LIANG Y. A., HSIEH S. T., ZESCH W., CHAN W. P., KENNY T. W. et al. Adhesive force of a single gecko foot-hair, Nature 2000: 405: 681-685.
3. GORB S. Attachment Devices of Insect Cuticle: Springer Netherlands; 2007.
4. ARZT E., GORB S., SPOLENAK R. From micro to nano contacts in biological attachment devices, Proceedings of the National Academy of Sciences 2003: 100: 10603-10606.
5. HUBER G., MANTZ H., SPOLENAK R., MECKE K., JACOBS K., GORB S. N. et al. Evidence for capillarity contributions to gecko adhesion from single spatula nanomechanical measurements, Proceedings of the National Academy of Sciences of the United States of America 2005: 102: 16293-16296.
6. HUBER G., GORB S. N., SPOLENAK R., ARZT E. Resolving the nanoscale adhesion of individual gecko spatulae by atomic force microscopy, Biology Letters 2005: 1: 2-4.
7. HUBER G., ORSO S., SPOLENAK R., WEGST U. G. K., ENDERS S., GORB S. N. et al. Mechanical properties of a single gecko seta, International Journal of Materials Research 2008: 99: 1113-1118.
8. HUBER G., GORB S. N., HOSODA N., SPOLENAK R., ARZT E. Influence of surface roughness on gecko adhesion, Acta biomaterialia 2007: 3: 607-610.
9. ORSO S., WEGST U. G. K., EBERL C., ARZT E. Micrometer-scale tensile testing of biological attachment devices, Advanced Materials 2006: 18: 874-+.
10. AUTUMN K., SITTI M., LIANG Y. A., PEATTIE A. M., HANSEN W. R., SPONBERG S. et al. Evidence for van der Waals adhesion in gecko setae, Proceedings of the National Academy of Sciences 2002: 99: 12252-12256.
11. AUTUMN K., DITTMORE A., SANTOS D., SPENKO M., CUTKOSKY M. Frictional adhesion: a new angle on gecko attachment, Journal of Experimental Biology 2006: 209: 3569-3579.
12. JIN K., TIAN Y., ERICKSON J. S., PUTHOFF J., AUTUMN K., PESIKA N. S. Design and Fabrication of Gecko-Inspired Adhesives, Langmuir 2012: 28: 5737-5742.

13. JAGOTA A., BENNISON S. J., SMITH C. A. Analysis of a compressive shear test for adhesion between elastomeric polymers and rigid substrates, International Journal of Fracture 2000: 104: 105-130.

14. JAGOTA A., BENNISON S. J. Mechanics of Adhesion Through a Fibrillar Microstructure, Integrative and Comparative Biology 2002: 42: 1140-1145.

15. SITTI M., FEARING R. S. Synthetic gecko foot-hair micro/nano-structures as dry adhesives, Journal of Adhesion Science and Technology 2003: 17: 1055-1073.

16. YURDUMAKAN B., RARAVIKAR N. R., AJAYAN P. M., DHINOJWALA A. Synthetic gecko foot-hairs from multiwalled carbon nanotubes, Chemical Communications 2005: 3799-3801.

17. HUI C.-Y., GLASSMAKER N. J., TANG T., JAGOTA A. Design of biomimetic fibrillar interfaces: 2. Mechanics of enhanced adhesion, Journal of The Royal Society Interface 2004: 1: 35-48.

18. GREINER C., DEL CAMPO A., ARZT E. Adhesion of Bioinspired Micropatterned Surfaces: Effects of Pillar Radius, Aspect Ratio, and Preload, Langmuir 2007: 23: 3495-3502.

19. DEL CAMPO A., GREINER C., ARZT E. Contact shape controls adhesion of bioinspired fibrillar surfaces, Langmuir 2007: 23: 10235-10243.

20. KIM S., SITTI M. Biologically inspired polymer microfibers with spatulate tips as repeatable fibrillar adhesives, Applied Physics Letters 2006: 89: 261911-261913.

21. GORB S., VARENBERG M., PERESSADKO A., TUMA J. Biomimetic mushroom-shaped fibrillar adhesive microstructure, Journal of the Royal Society, Interface / the Royal Society 2007: 4: 271-275.

22. PARETKAR D., KAMPERMAN M., MARTINA D., ZHAO J., CRETON C., LINDNER A. et al. Preload-responsive adhesion: effects of aspect ratio, tip shape and alignment, Journal of the Royal Society Interface 2013: 10.

23. MICCICHÉ M., ARZT E., KRONER E. Single Macroscopic Pillars as Model System for Bioinspired Adhesives: Influence of Tip Dimension, Aspect Ratio, and Tilt Angle, ACS applied materials & interfaces 2014: 6: 7076-7083.

24. CANAS N., KAMPERMAN M., VOLKER B., KRONER E., MCMEEKING R. M., ARZT E. Effect of nano- and micro-roughness on adhesion of bioinspired micropatterned surfaces, Acta biomaterialia 2012: 8: 282-288.

25. PERSSON B. N. J., TOSATTI E. The effect of surface roughness on the adhesion of elastic solids, The Journal of chemical physics 2001: 115: 5597-5610.

26. PERSSON B. N. J., GORB S. The effect of surface roughness on the adhesion of elastic plates with application to biological systems, The Journal of chemical physics 2003: 119: 11437-11444.

27. KIM S., SITTI M., HUI C.-Y., LONG R., JAGOTA A. Effect of backing layer thickness on adhesion of single-level elastomer fiber arrays, Applied Physics Letters 2007: 91: -.

28. LONG R., HUI C.-Y., KIM S., SITTI M. Modeling the soft backing layer thickness effect on adhesion of elastic microfiber arrays, Journal of Applied Physics 2008: 104: 044301-044309.

29. GAO H., WANG X., YAO H., GORB S., ARZT E. Mechanics of hierarchical adhesion structures of geckos, Mechanics of Materials 2005: 37: 275-285.

30. YAO H., GAO H. Mechanics of robust and releasable adhesion in biology: Bottom–up designed hierarchical structures of gecko, Journal of the Mechanics and Physics of Solids 2006: 54: 1120-1146.

31. GLASSMAKER N. J., JAGOTA A., HUI C. Y. Adhesion enhancement in a biomimetic fibrillar interface, Acta biomaterialia 2005: 1: 367-375.

32. GLASSMAKER N. J., JAGOTA A., HUI C.-Y., KIM J. Design of biomimetic fibrillar interfaces: 1. Making contact, Journal of The Royal Society Interface 2004: 1: 23-33.

33. SPUSKANYUK A. V., MCMEEKING R. M., DESHPANDE V. S., ARZT E. The effect of shape on the adhesion of fibrillar surfaces, Acta biomaterialia 2008: 4: 1669-1676.

34. AKSAK B., HUI C. Y., SITTI M. The effect of aspect ratio on adhesion and stiffness for soft elastic fibres, Journal of the Royal Society, Interface / the Royal Society 2011: 8: 1166-1175.

35. AKSAK B., SAHIN K., SITTI M. The optimal shape of elastomer mushroom-like fibers for high and robust adhesion, Beilstein Journal of Nanotechnology 2014: 5: 630-638.

36. CARBONE G., PIERRO E. Sticky bio-inspired micropillars: finding the best shape, Small (Weinheim an der Bergstrasse, Germany) 2012: 8: 1449-1454.

37. KHADERI S. N., FLECK N. A., ARZT E., MCMEEKING R. M. Detachment of an adhered micropillar from a dissimilar substrate, Journal of the Mechanics and Physics of Solids 2014.

38. AKISANYA A. R., FLECK N. A. Interfacial cracking from the freeedge of a long bi-material strip, International Journal of Solids and Structures 1997: 34: 1645-1665.

39. ABAQUS 6.11 Documentation: Dassault Systems, Simulia Corporation, Providence, Rhode Island, USA.

40. HOSSFELD C. K., SCHNEIDER A. S., ARZT E., FRICK C. P. Detachment Behavior of Mushroom-Shaped Fibrillar Adhesive Surfaces in Peel Testing, Langmuir 2013: 29: 15394-15404.

Figures

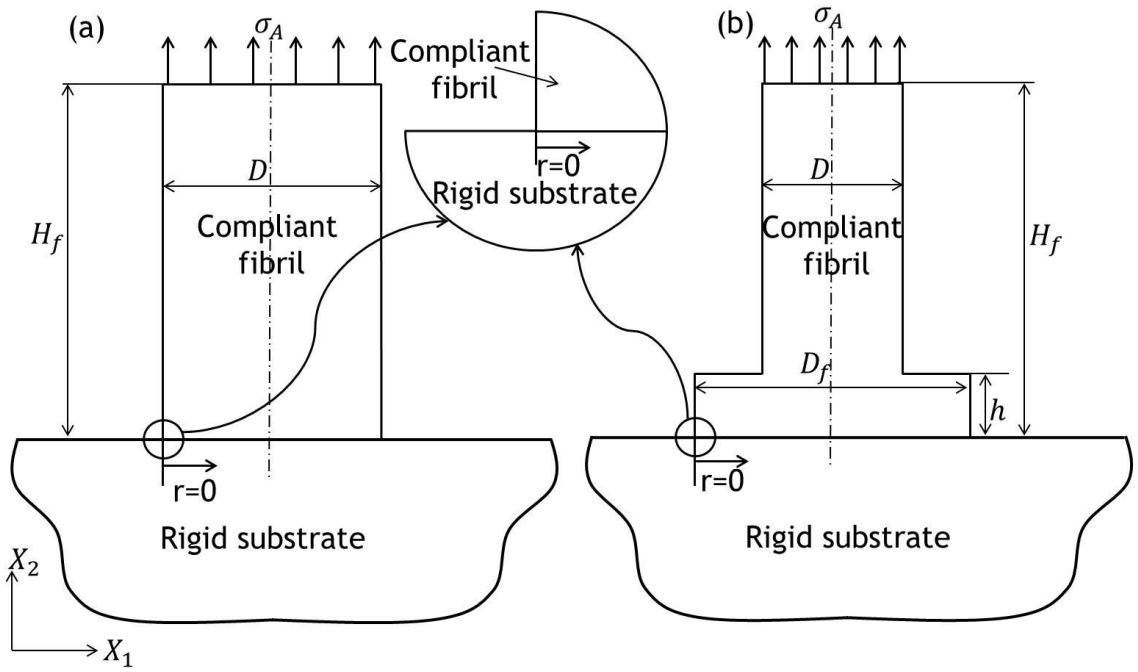

Figure 1: Schematics of (a) a straight punch shaped fibril without a mushroom cap and (b) a fibril with a mushroom cap, both adhered to a rigid substrate.

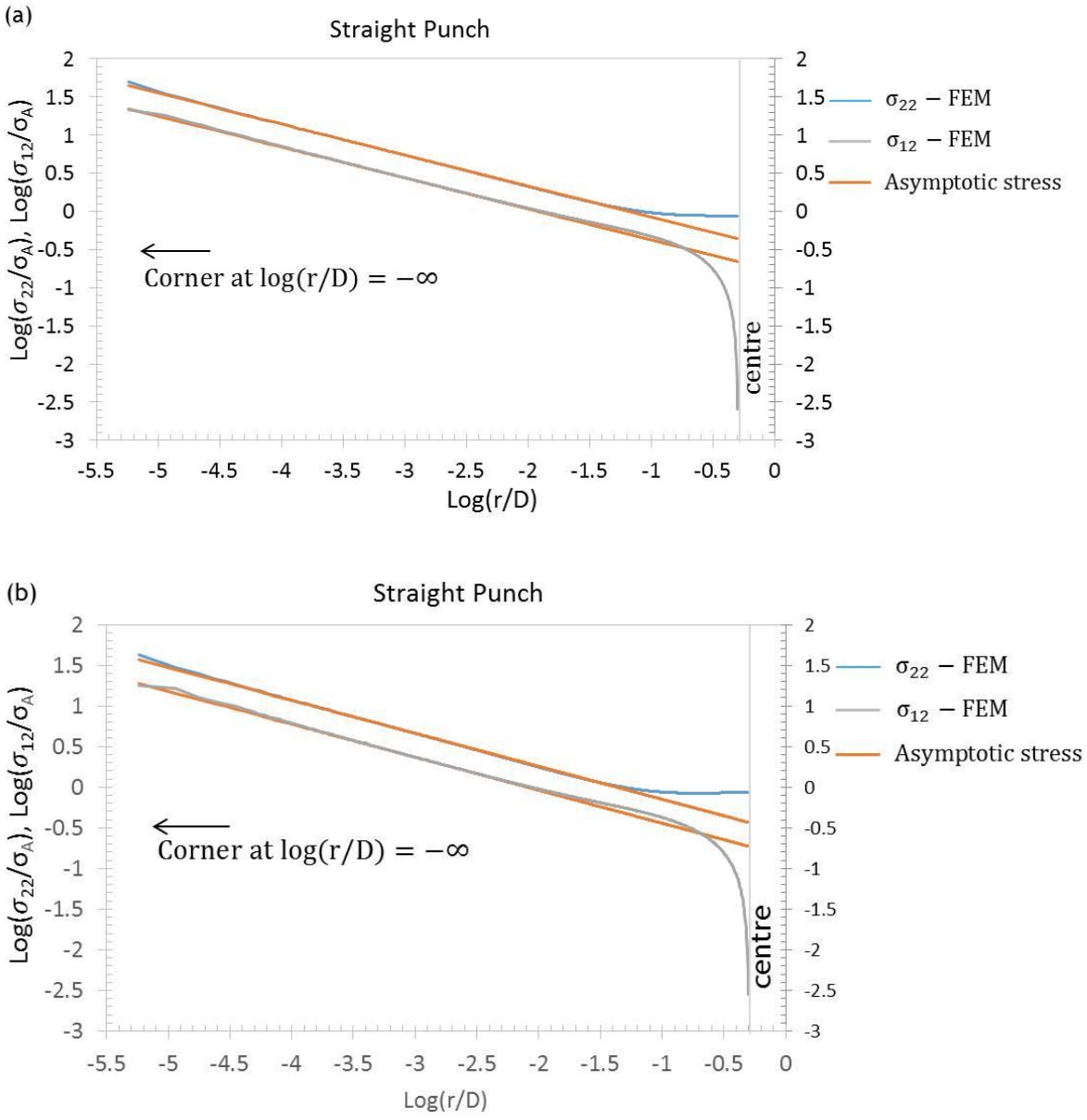

Figure 2: Normalised normal (σ_{22}) and shear (σ_{12}) tractions for the straight punch (corner to centre) for (a) plane strain and (b*)* axial symmetry. The remote applied stress is denoted by σ_A.

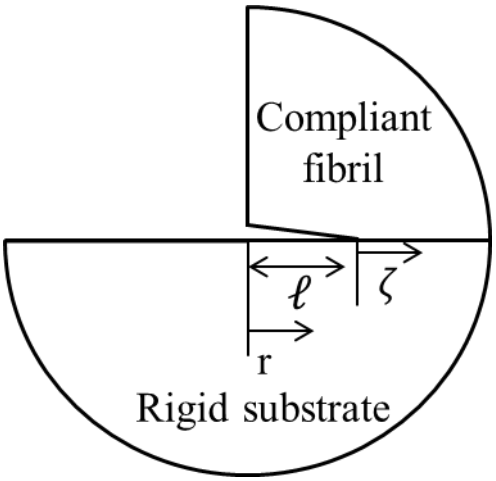

Figure 3: Schematic of a small crack along the interface at the corner of the contact.

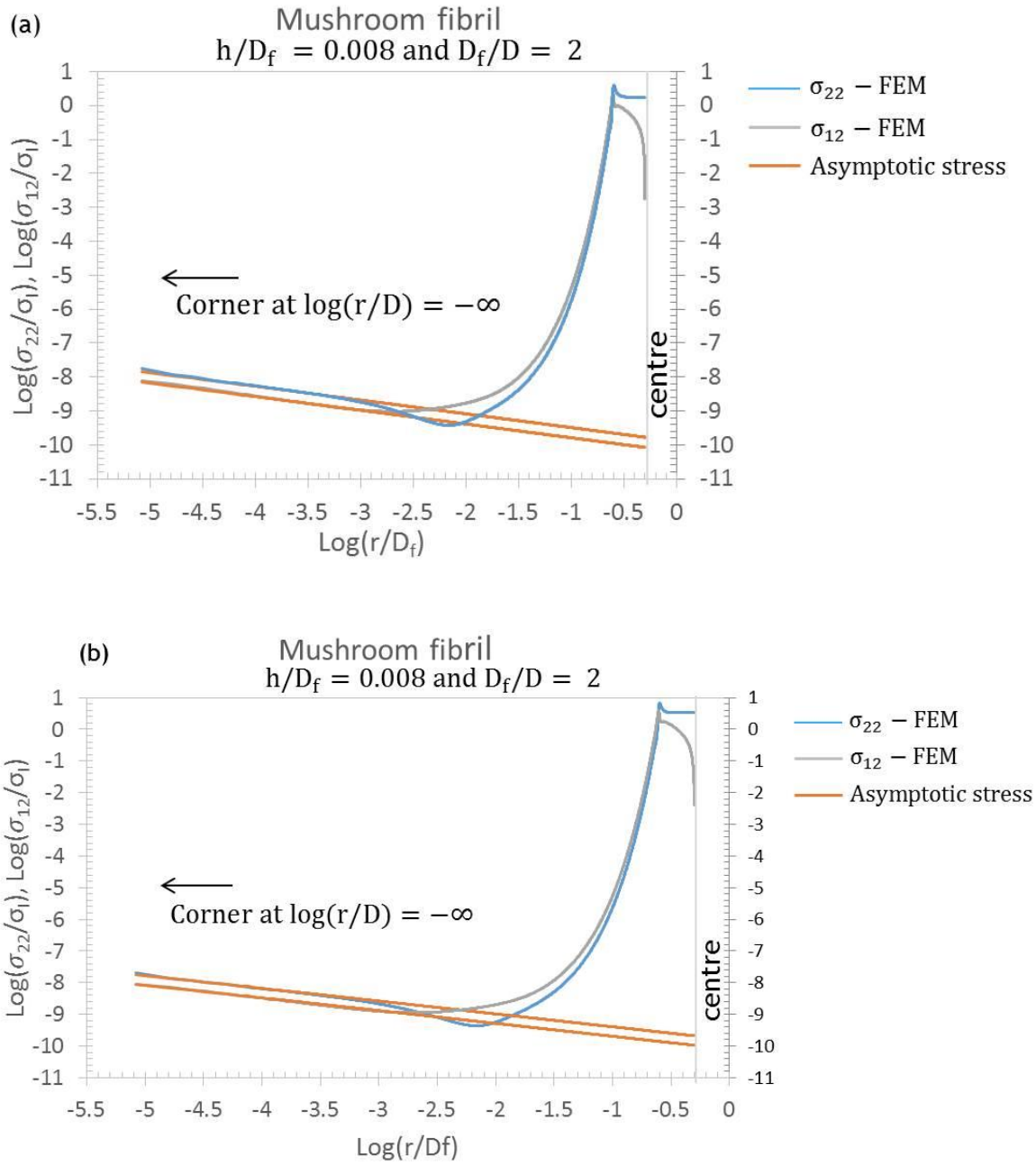

Figure 4: Comparison of the finite element results and the theoretical asymptotic results for the normal and shear tractions on the interface between the substrate and a specific mushroom capped fibril. The results are plotted from near the edge (left) to the fibril centre (right) for (a) plane strain and (b) axial symmetry.

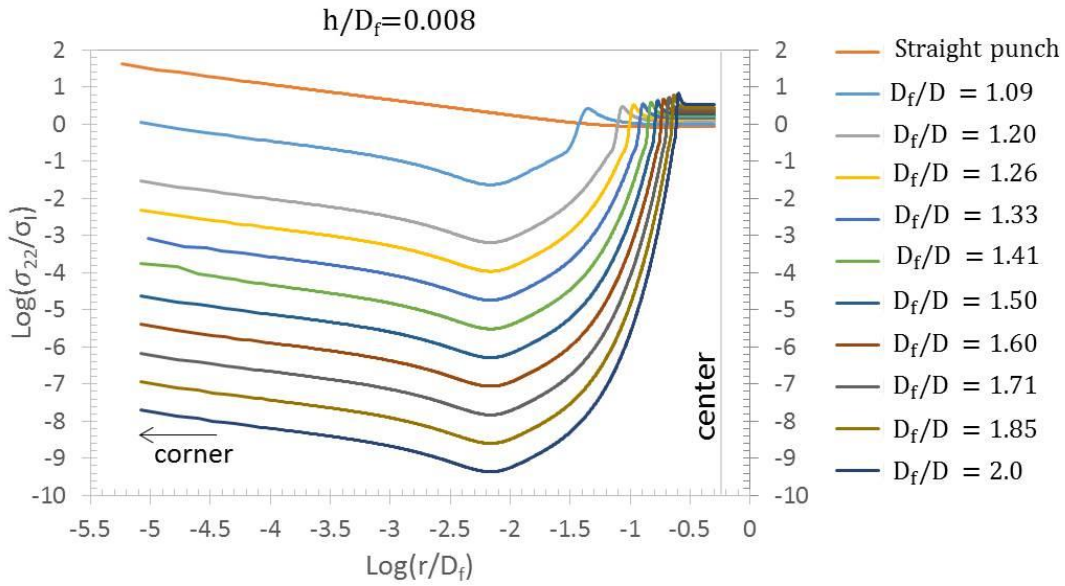

Figure 5: Tensile stress along the interface between the substrate and a fibril having a mushroom cap for axial symmetry for various values of the mushroom cap diameter, D_f, divided by the diameter, D, of the fibril stalk. Results are shown for a mushroom cap that has a thickness, h, equal to 0.008 times its diameter.

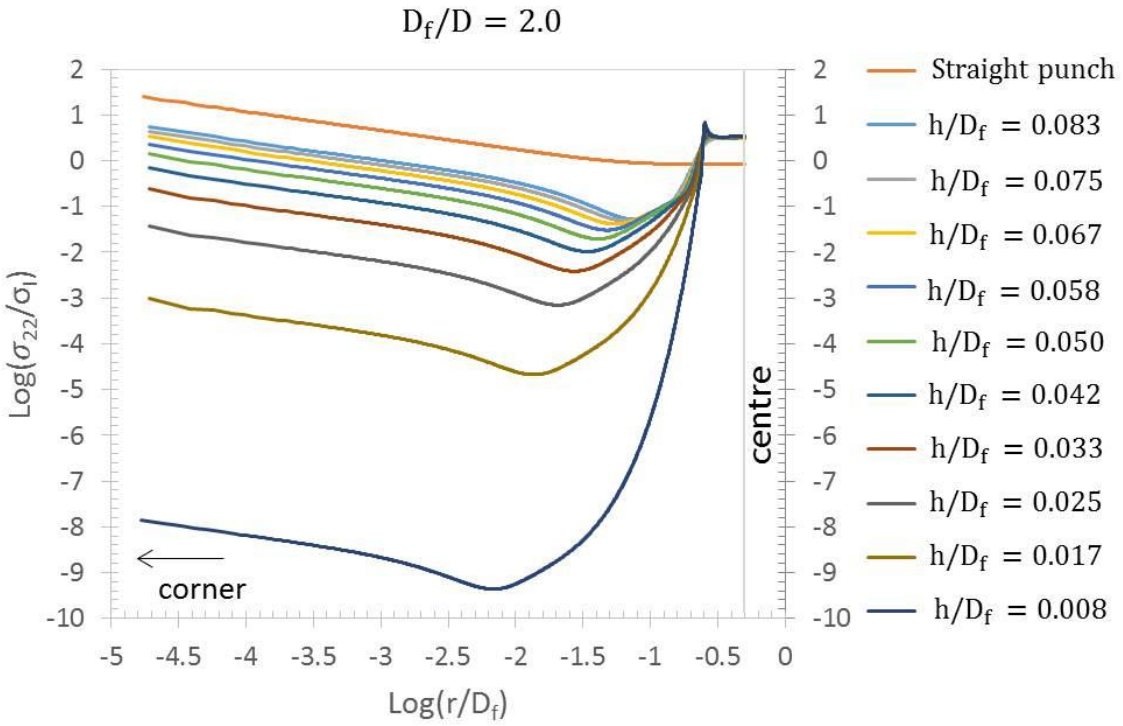

Figure 6: Tensile stress along the interface between the substrate and a fibril having a mushroom cap for axial symmetry for various values of the ratio of the cap thickness to its diameter h/D_f. Results are shown for a fibril having a mushroom cap whose diameter is twice that of its stalk.

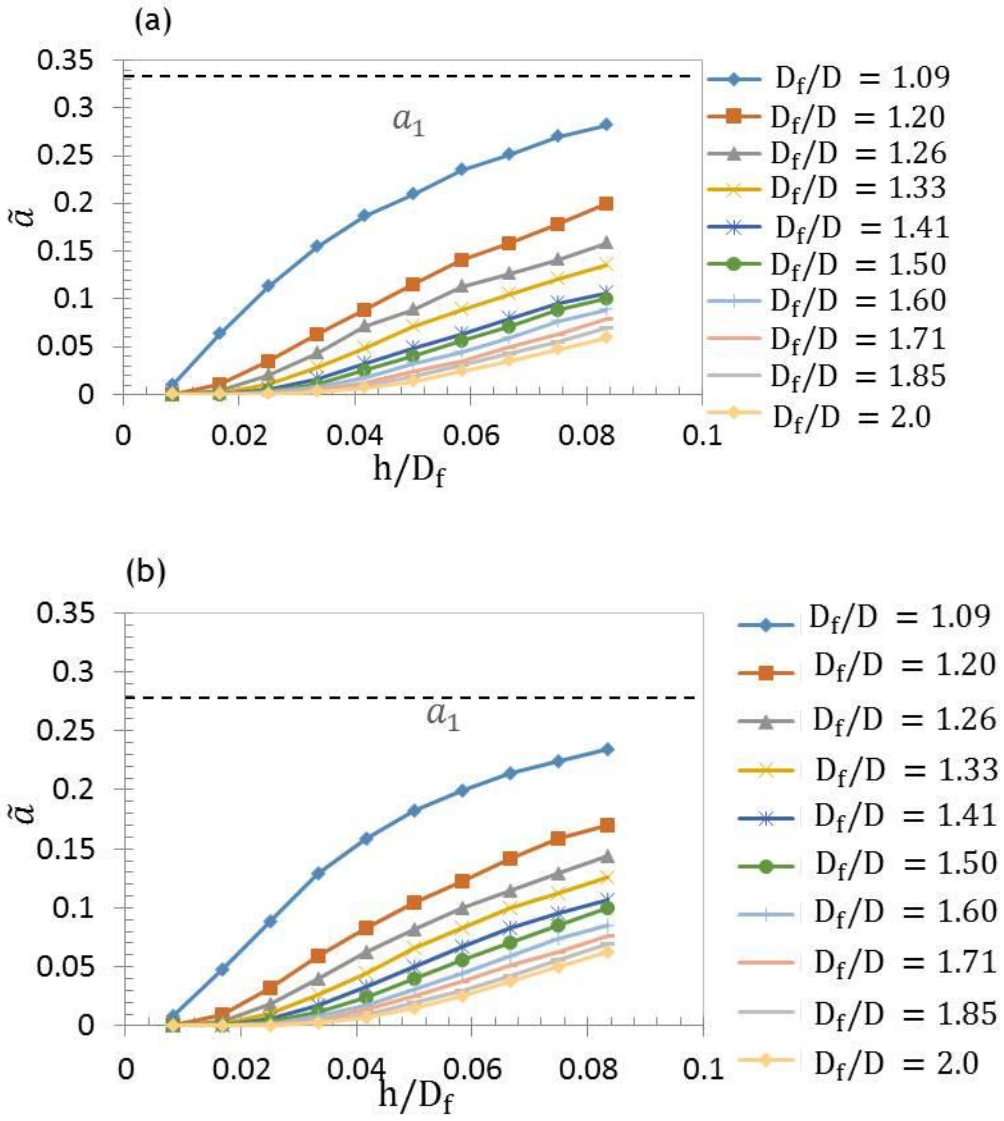

Figure 7: Calibration coefficient, $\tilde{a}$, plotted as a function of the ratio of mushroom cap thickness to diameter, h/D_f, for various ratios of fibril mushroom cap diameter to fibril stalk diameter D_f/D for (a) plane strain and (b) axial symmetry. The dashed horizontal lines indicate the value of the calibration coefficients a_1 for a straight punch.

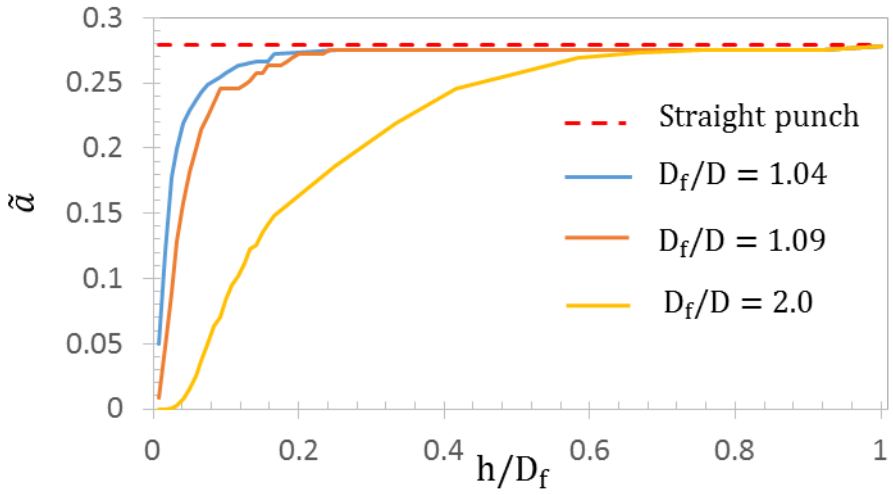

Figure 8: Calibration coefficient $\tilde{a}$ plotted as a function of the ratio of mushroom cap thickness to diameter, h/D_f, for 3 values of the ratio of fibril mushroom cap diameter to fibril stalk diameter D_f/D for axial symmetry. The dashed horizontal lines indicate the value of the calibration coefficient a_1 for a straight punch. The plot is extended to $h/D_f = 1$ to show how the results for the mushroom capped fibril converge to that of the straight punch as the mushroom cap is thickened.

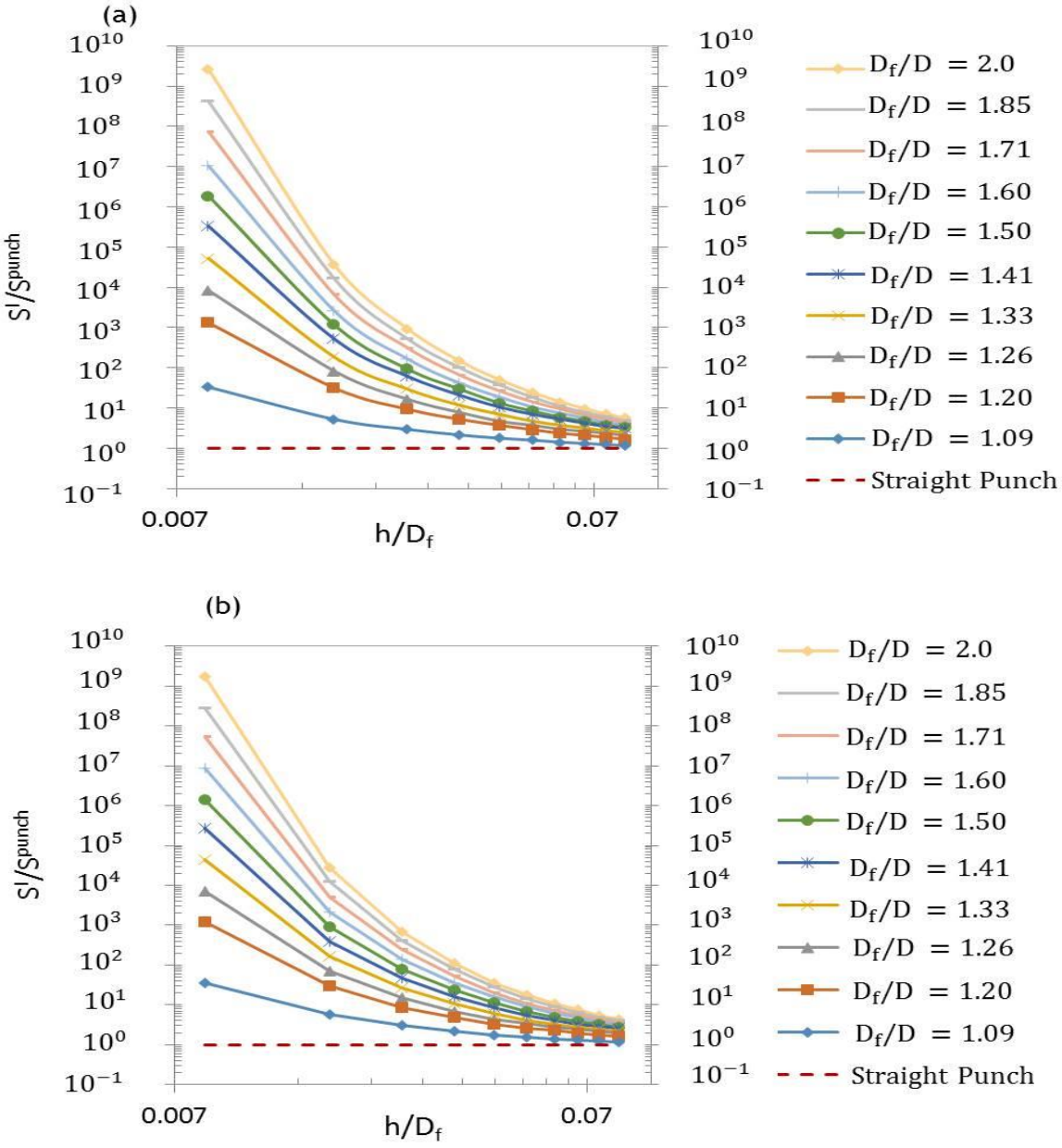

Figure 9: Adhesion strength for edge initiated detachment for a fibril having a mushroom cap of thickness h and diameter D_f is shown for (a) plane strain and (b) axial symmetry. The adhesion strength, S^I, of the fibril with the mushroom cap is given in terms of the average stress on the interface and is normalised by the adhesion strength, S^{punch} of a straight punch fibril having the same diameter as the mushroom cap, with Young's modulus, adhesion energy and edge detachment length, l, the same for all fibrils.

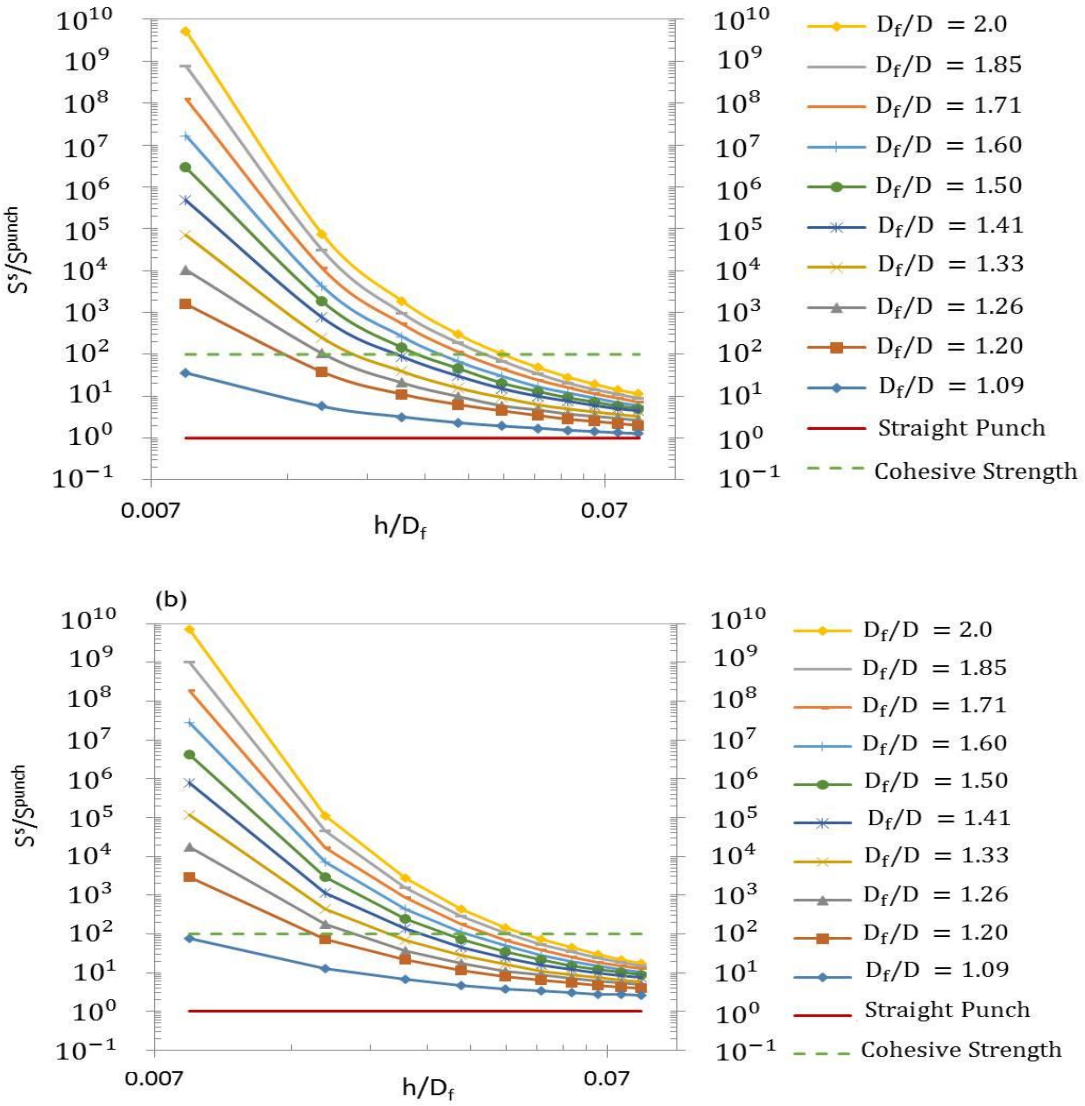

Figure 10: Adhesion strength, S^S (full lines), for for edge initiated detachment fibrils having mushroom caps of thickness h and diameter D_f is plotted for (a) plane strain and (b) axial symmetry. In this case the adhesion strength is given in terms of the average stress applied to the mushroom fibril stalk of diameter D and is normalised by the adhesion strength, S^{punch}, for a straight punch fibril having the same diameter as the mushroom cap, with Young's modulus, adhesion energy and edge detachment length, l, the same for all fibrils. The detachment strength associated with the stress under the stalk reaching a critical value S^C is represented by the horizontal dashed lines, marked "Cohesive Strength S^C."

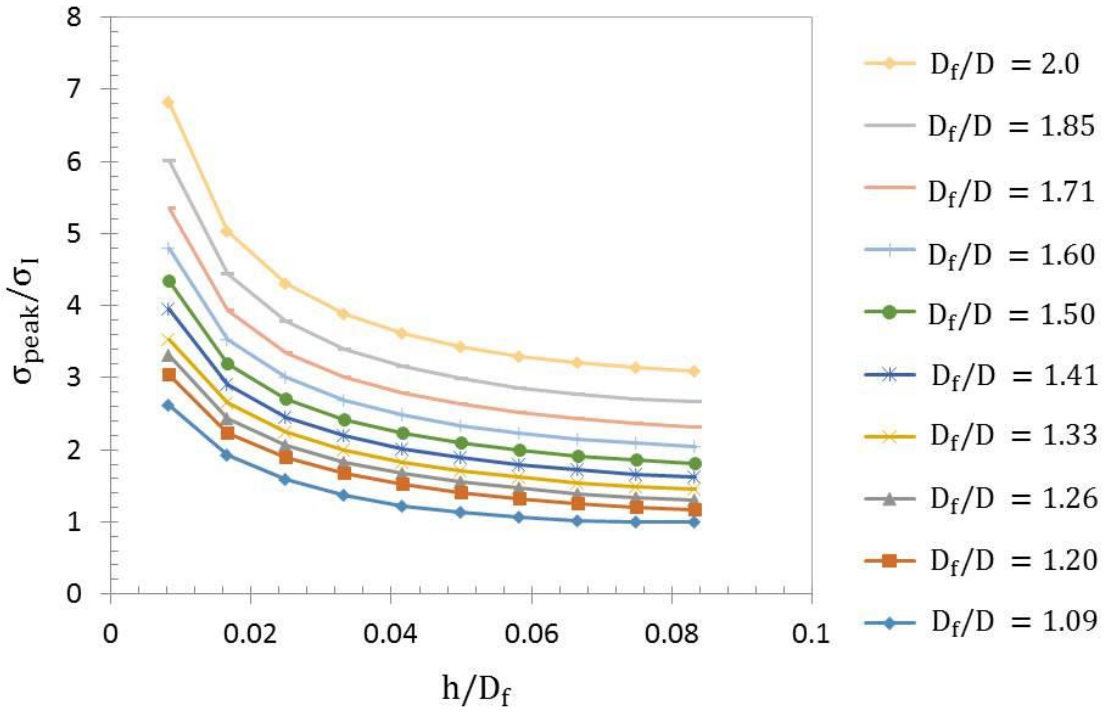

Figure 11: The magnitude of the local peak stress σ_{peak} near the centre of the fibril as depicted in the plots of interface stress in Figure 5 and Figure 6. The peak stress is normalised by the average interface stress σ_I and is therefore given as the stress concentration factor k. The result is shown as a function of h/D_f for various values of D_f/D. Note that a thin mushroom cap and a thin stalk will promote detachment at the centre by raising the local peak stress there.

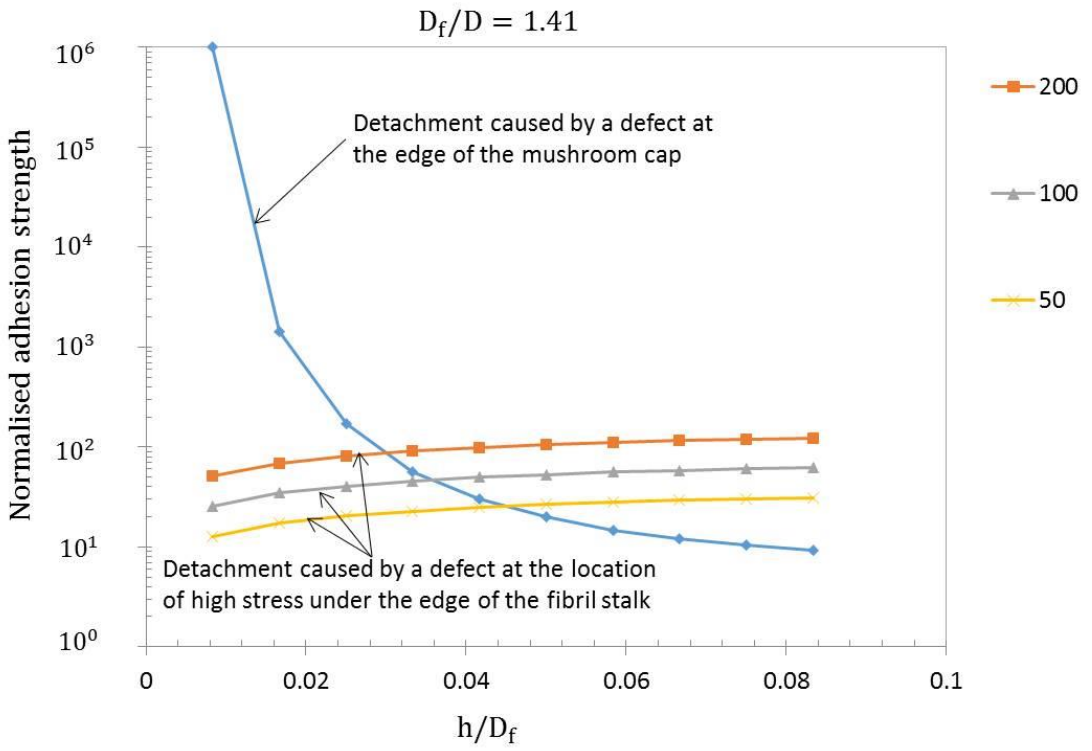

Figure 12: Adhesion strength for a fibril having a mushroom cap predicted for detachment due to a defect at the edge of the mushroom cap ($\overline{S}^I$) and for detachment due to a defect at the location of high stress under the edge of the fibril stalk ($\overline{S}^P$). The ratio of fibril mushroom cap diameter to fibril stalk diameter $D_f/D = 1.41$ and the fibril is axisymmetric. The defect sizes are plotted for three different values of $(3.3D_f^{0.406}\ l^{0.094})/\sqrt{1.5\pi a} = 50, 100,$ and 200 where l is the size of the defect at the mushroom cap edge and $2a$ is the size of the defect at the location of the high stress. These curves are marked accordingly as $50, 100$ and 200.

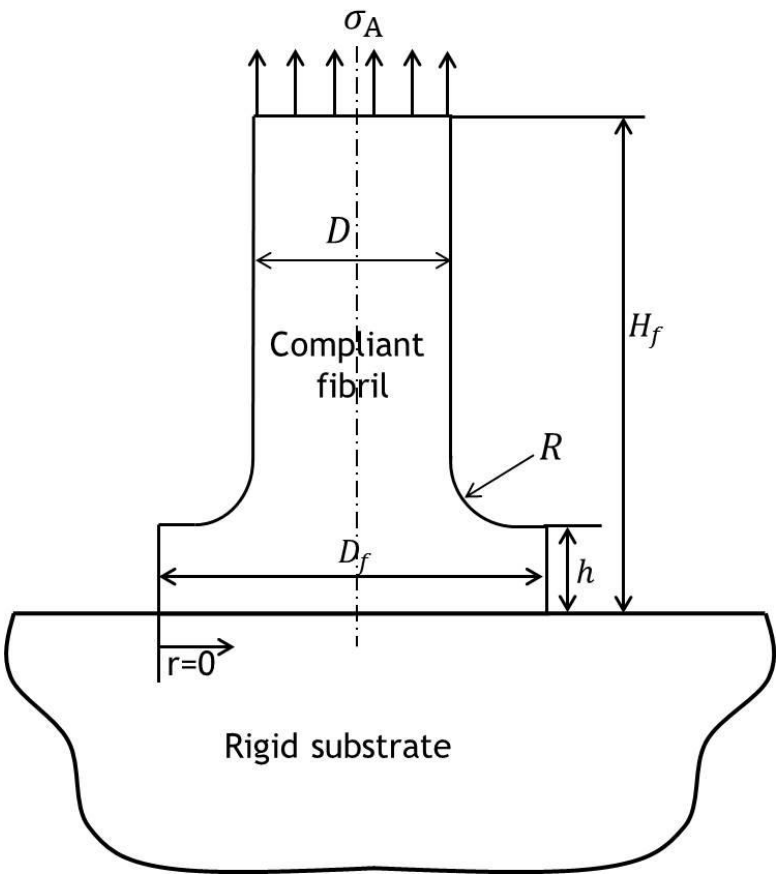

Figure 13: Schematic of a mushroom fibril with a fillet of radius R where $R/D_f = 0.083$.

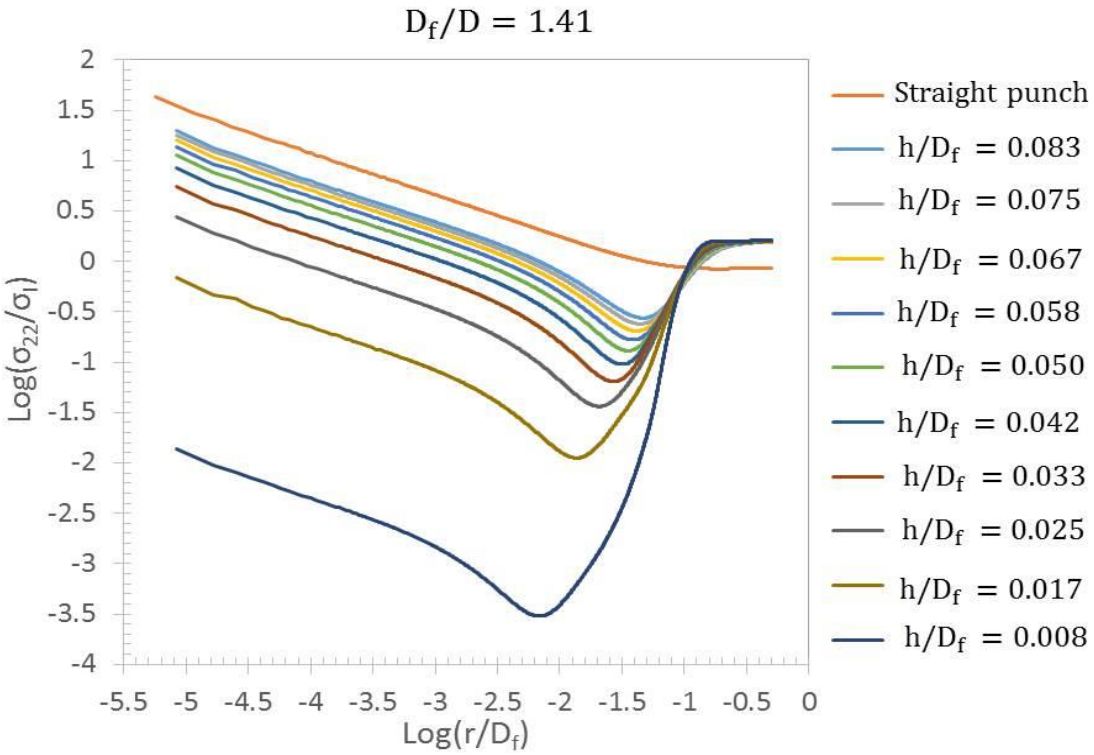

Figure 14: Tensile stress along the interface between the substrate and an axisymmetric mushroom cap fibril having a value of the radius of the fillet, R, that is effective at eliminating the high stress under the edge of the fibril stalk. Results are shown for a fibril having a mushroom cap whose diameter is 1.41 times that of its stalk and for various values of the ratio of the cap thickness to its diameter h/D_f. The fillet radius is such that $R/D_f = 0.083$.

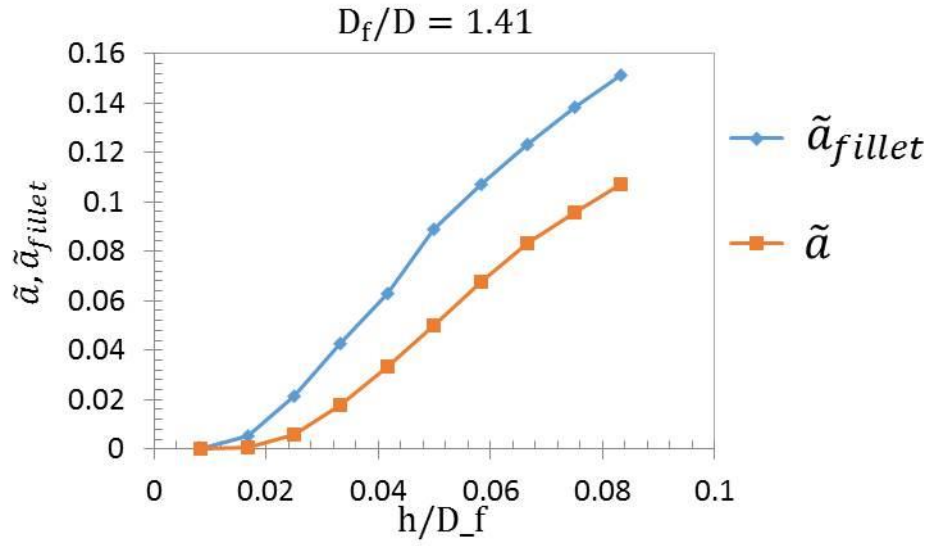

Figure 15: Calibration coefficients, $\tilde{a}$, for mushroom fibrils without fillet radii and, $\tilde{a}_{fillet}$, for mushroom fibrils with fillet radii, both plotted as a function of the ratio of mushroom cap thickness to diameter, h/D_f, for a ratio of fibril mushroom cap diameter to fibril stalk diameter $D_f/D = 1.41$ for axisymmetric fibrils. The fillet radius is such that $R/D_f = 0.083$.

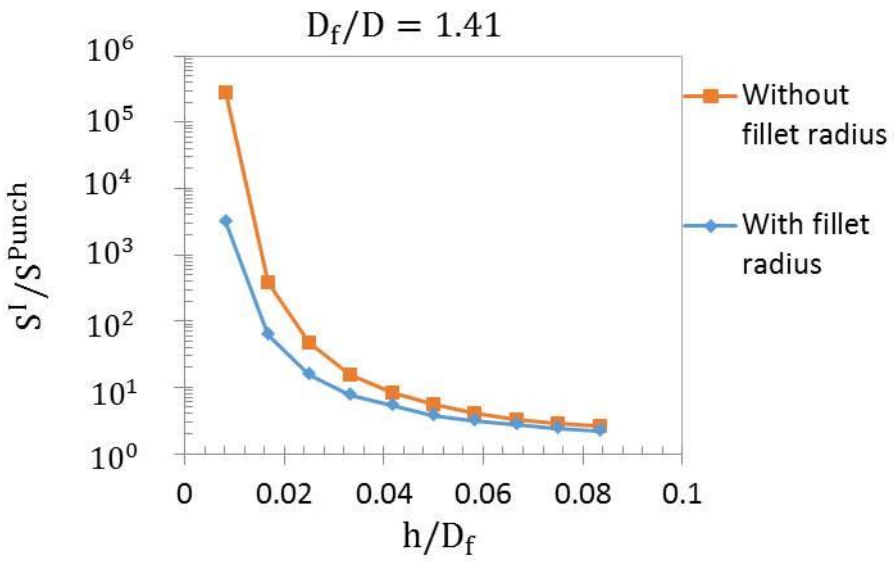

Figure 16: Adhesion strength for fibrils with and without fillet radii plotted versus h/D_f for a ratio of fibril mushroom cap diameter to fibril stalk diameter $D_f/D = 1.41$ for axisymmetric mushroom fibrils. Detachment in these cases is initiated at the edge of the mushroom cap. The adhesion strength is normalised by that for a punch shaped fibril. The fillet radius is such that $R/D_f = 0.083$

Tables

	D_f/D									
h/D_f	1.09	1.2	1.26	1.33	1.41	1.50	1.6	1.71	1.85	2
0.008	0.010	2.5E-04	4.0E-05	6.3E-06	1E-06	1.8E-07	3.2E-08	4.5E-09	7.9E-10	1.3E-10
0.017	0.063	0.010	4.0E-03	1.78E-03	6.3E-04	2.82E-04	1.26E-04	5.0E-05	2E-05	8.9E-06
0.025	0.112	0.035	0.020	0.011	0.0054	0.004	0.002	0.0011	0.0006	0.0004
0.033	0.155	0.063	0.043	0.028	0.0158	0.011	0.0079	0.0050	0.003	0.002
0.042	0.186	0.089	0.071	0.048	0.0316	0.025	0.0178	0.0126	0.009	0.007
0.050	0.209	0.115	0.089	0.071	0.0479	0.040	0.0316	0.0234	0.018	0.014
0.058	0.234	0.141	0.112	0.089	0.0631	0.056	0.0447	0.0355	0.030	0.023
0.067	0.251	0.158	0.126	0.105	0.0794	0.071	0.0589	0.0501	0.043	0.035
0.075	0.269	0.178	0.141	0.120	0.0955	0.089	0.0759	0.0631	0.055	0.047
0.083	0.282	0.200	0.158	0.135	0.1059	0.1	0.0891	0.079	0.069	0.059

Table 1: Calibration coefficients $\tilde{a}$ for plane strain fibrils having a mushroom cap of width D_f and thickness h. The width of the fibril stalk is D.

	D_f/D									
h/D_f	1.09	1.20	1.26	1.33	1.41	1.50	1.60	1.71	1.85	2.0
0.008	0.008	2.2E-04	4.0E-05	6.3E-06	1.0E-06	2.0E-07	3.2E-08	5.0E-09	1.0E-09	1.6E-10
0.017	0.048	0.009	4.0E-03	1.7E-03	7.1E-04	3.0E-04	1.3E-04	5.6E-05	2.2E-05	1.0E-05
0.025	0.089	0.032	0.019	0.010	0.006	0.004	0.002	0.0011	0.0007	0.0004
0.033	0.129	0.059	0.040	0.0263	0.018	0.012	0.008	0.005	0.0035	0.003
0.042	0.158	0.083	0.063	0.045	0.033	0.025	0.018	0.013	0.010	0.008
0.050	0.182	0.105	0.081	0.066	0.050	0.040	0.031	0.025	0.019	0.015
0.058	0.200	0.123	0.100	0.083	0.068	0.056	0.045	0.038	0.030	0.025
0.067	0.214	0.141	0.115	0.100	0.083	0.071	0.059	0.051	0.043	0.037
0.075	0.224	0.158	0.129	0.112	0.095	0.085	0.074	0.063	0.056	0.050
0.083	0.234	0.170	0.145	0.126	0.107	0.1	0.085	0.076	0.069	0.063

Table 2: Calibration coefficients $\tilde{\alpha}$ for axially symmetric fibrils having a mushroom cap of diameter D_f, and thickness h where D is the diameter of the fibril stalk.

h/D_f	$\tilde{a}_{fillet}$	S^I_{fillet}/S^{Punch}
0.0083	1.05E-04	3.16E+03
0.0167	5.25E-03	6.31E+01
0.0250	2.14E-02	1.55E+01
0.0333	4.27E-02	7.76E+00
0.0417	6.31E-02	5.25E+00
0.0500	8.91E-02	3.71E+00
0.0583	1.07E-01	3.09E+00
0.0667	1.23E-01	2.69E+00
0.0750	1.38E-01	2.40E+00
0.0833	1.51E-01	2.19E+00

Table 3: Calibration coefficients ã for axisymmetric fibrils having a fillet radius that is effective at eliminating the high stress under the fibril stalk for mushroom caps with $D_f/D = 1.41$ where D_f and D are the diameter of mushroom cap and the stalk respectively and h is the thickness of the mushroom cap. The fillet radius $R/D_f = 0.083$.

6 Supplementary section

6.1 Mushroom Fibrils (plane strain results)

The plane strain results for mushroom fibrils are in good agreement with the asymptotic solution and are similar to those for axisymmetric fibrils. Some of the plane strain results are therefore not listed in the main paper and are provided here. The influence of the stalk diameter D and the mushroom cap height h on the stress along the interface between a compliant fibril and a substrate is shown in Figure S1 (in analogy with axisymmetric results in Figure 5) and Figure S2 (in analogy with axisymmetric results in Figure 6).

[Figure S1 will be here]

[Figure S2 will be here]

Supplementary Figures

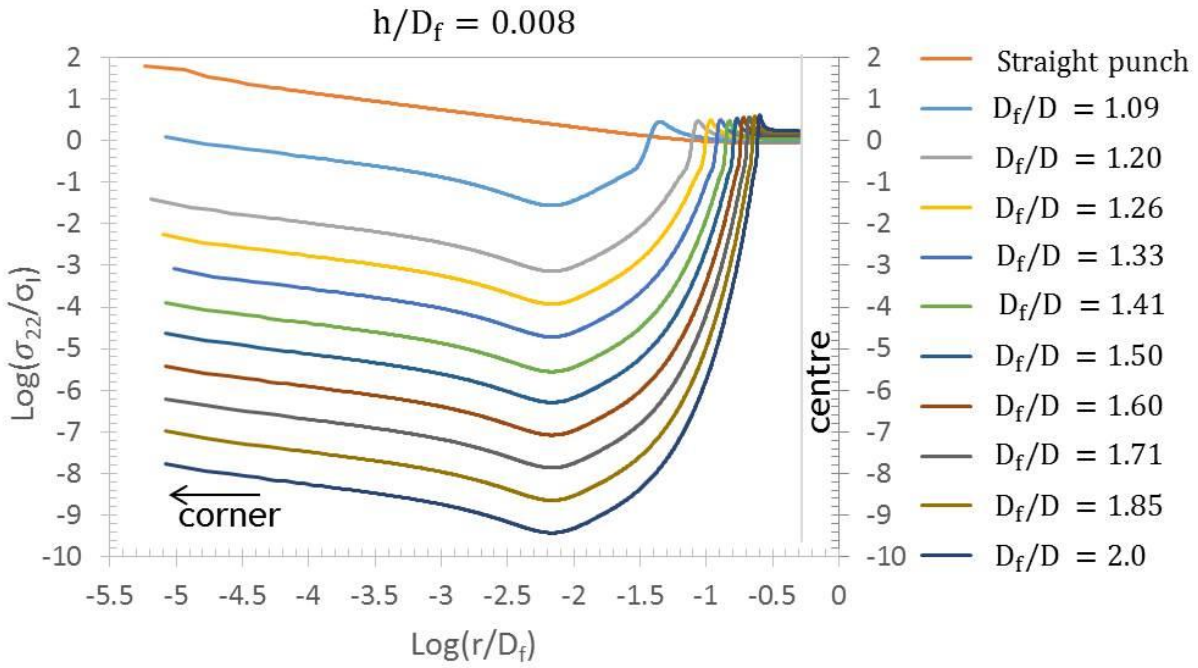

Figure S1: Tensile stress along the interface between the substrate and a fibril having a mushroom cap for plane strain for various values of the mushroom cap width, D_f, divided by the width, D, of the fibril stalk. Results are shown for a mushroom cap that has a thickness, h, equal to 0.008 times its width.

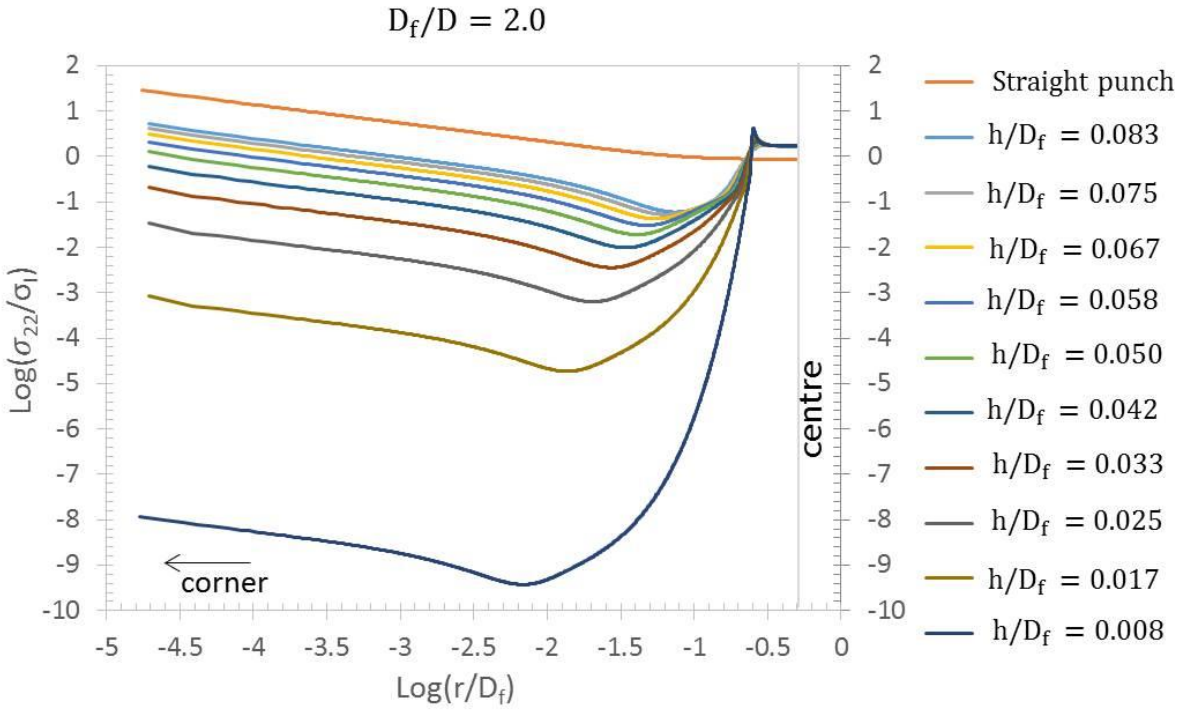

Figure S2: Tensile stress along the interface between the substrate and a fibril having a mushroom cap for plane strain for various values of the ratio of the cap thickness to its width h/D_f. Results are shown for a fibril having a mushroom cap whose diameter is twice that of its stalk.